Measurement of the magnetic fine structure of the $10G$ and $10H$ states of helium

E. A. Hessels, W. G. Sturrus, and S. R. Lundeen
Department of Physics, University of Notre Dame, Notre Dame, Indiana 46556

David R. Cok
Eastman Kodak Company Research Laboratories, Rochester, New York 14650
(Received 18 November 1986)

The magnetic fine-structure intervals separating the four members of the $10G$ and $10H$ manifolds of helium have been measured with a precision of 0.1% using a fast-beam microwave-optical resonance technique. The results are found to be in good agreement with theory, illustrating that the two-electron wave function is very nearly hydrogenic. The measurements are also used to determine the small exchange energies of the $10G$ and $10H$ states.

I. INTRODUCTION

The high-angular-momentum Rydberg states of helium are unique among two-electron states for the simplicity of their wave functions. Both the highly excited Rydberg electron in its nonpenetrating high-L orbit and the tightly bound core ($1s$) electron are described very accurately by hydrogenic wave functions. As a result, the binding energies of these states can be understood with great precision and can be used to test for subtle effects in the electron-electron interaction.[1,2] When electron spin is included, each high-L configuration consists of four energy levels which are nearly equally spaced, as illustrated for the $10G$ and $10H$ states in Fig. 1. It is this structure that we refer to as magnetic structure. The four sublevels are labeled according to the standard LS coupling scheme $^{2S+1}L_J$, except that the two levels with $J=L$, which are approximately equal mixtures of singlet and triplet states, are labeled $^{\pm}L_J$ to emphasize the spoiling of the total electronic spin quantum number.[3] To date, this structure has not been studied nearly as carefully as the electric fine structure which separates states of different L.[4,5] The most precise theoretical treatment of the magnetic structure has been carried out by Cok,[6] who also surveyed the existing experimental data relevant to these structures. Cok calculated that the portion of the magnetic structure due to corrections to the lowest-order hydrogenic wave function decreases rapidly with L; however, rather poor agreement between predicted and observed structures in G states left open the question as to whether the high-L structure was correctly described. Recent calculations have suggested other contributions to the structure, which must be added to those described by Cok.[7] The measurements reported here significantly improve experimental knowledge in this area.

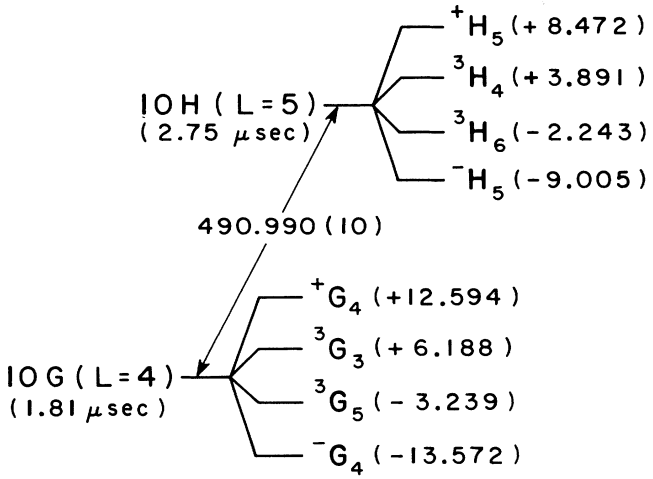

FIG. 1. Energy-level diagram for the $10G$ and $10H$ states. The value of the electric-fine-structure splitting is that measured by Palfrey (Ref. 1). The values of the magnetic-fine-structure splittings are calculated using the theory described in the text and our measured $10G$ exchange energy. The states are labeled $^{2S+1}L_J$ except for the two states with $J=L$, $^{\pm}L_J$, which are approximately equal mixtures of singlet and triplet states.

II. THEORY

Each singly excited helium configuration consists of four nearly degenerate energy levels. The two effects that contribute to the splittings between these levels are the exchange energy, which results from symmetrizing the spatial wave function, and the explicitly spin-dependent interactions. For low-L states, the exchange energy dominates and, as a result, the structure consists of an isolated singlet and a closely spaced triplet, which correspond to spatial wave functions of even and odd exchange symmetry, respectively. For high L ($L>3$), the exchange energy becomes very small and the spin-dependent interactions dominate the structure, leading to the pattern of four nearly equally spaced levels.

This structure may be described within a nonrelativistic framework by taking as the Hamiltonian

$$H=H_{\text{Coulomb}}+H_{\text{spin}}\ , \tag{1}$$

where H_{Coulomb} is the nonrelativistic Coulomb Hamiltoni-

an for the helium atom and H_{spin} contains the spin-dependent interactions. H_{Coulomb} is conveniently written in terms of the coordinates $\mathbf{r}_1$ and $\mathbf{r}_2$ that measure the position of each electron relative to the nucleus. Neglecting the center-of-mass energy and the mass-polarization term produced in this transformation, and writing the remaining Hamiltonian in a form appropriate for Rydberg states, we have

$$H_{\text{Coulomb}}=H_0+V\ , \tag{2}$$

where (in atomic units, $e=\hbar=m_e=1$)

$$H_0=-(\,|\,\mathbf{p}_1\,|^2/2\mu-2/|\,\mathbf{r}_1\,|\,)+(\,|\,\mathbf{p}_2\,|^2/2\mu-1/|\,\mathbf{r}_2\,|\,)$$

and

$$V=1/|\,\mathbf{r}_{12}\,|-1/|\,\mathbf{r}_2\,|\ ,$$

with $\mu=mM/(m+M)$ and $\mathbf{r}_{12}=\mathbf{r}_1-\mathbf{r}_2$. In this paper, we treat only the hydrogenic model of the magnetic fine structure, based on the zeroth-order eigenfunctions of H_{Coulomb}, which are eigenfunctions of H_0. Corrections to this simple hydrogenic model have been calculated by Cok.[6]

H_{spin} is given, to lowest order, by the nonrelativistic reduction of the Breit interaction.[8] For measurements of the precision reported here, it is necessary to improve this approximation by adding corrections of order αH_{spin} due to the electron's anomalous magnetic moment.[9] It is also a simple matter to include those corrections of order $(m/M)H_{\text{spin}}$, due to the motion of the (finite mass) nucleus, that have been discussed by Douglas.[10] This leads to the spin Hamiltonian given by Cok,[6] which can also be written (in atomic units) as

$$\begin{aligned}H_{\text{spin}}=&\alpha^2\left[\frac{\mathbf{r}_2\times\mathbf{p}_2}{r_2^3}\cdot\mathbf{S}_2+\frac{\mathbf{r}_1\times\mathbf{p}_1}{r_1^3}\cdot\mathbf{S}_1\right][(g-1)+gm/M]+\alpha^2\left[\frac{\mathbf{r}_{12}\times\mathbf{p}_2}{2r_{12}^3}\cdot\mathbf{S}_2-\frac{\mathbf{r}_{12}\times\mathbf{p}_1}{2r_{12}^3}\cdot\mathbf{S}_1\right](g-1)\\&+\alpha^2\left[\frac{\mathbf{r}_{12}\times\mathbf{p}_2}{r_{12}^3}\cdot\mathbf{S}_1-\frac{\mathbf{r}_{12}\times\mathbf{p}_1}{r_{12}^3}\cdot\mathbf{S}_2\right](g/2)+\alpha^2\left[\frac{\mathbf{S}_1\cdot\mathbf{S}_2-3(\mathbf{S}_1\cdot\hat{\mathbf{r}}_{12})(\hat{\mathbf{r}}_{12}\cdot\mathbf{S}_2)}{r_{12}^3}-(8\pi/3)\delta^{(3)}(\mathbf{r}_{12})\mathbf{S}_1\cdot\mathbf{S}_2\right](g/2)^2\ ,\end{aligned} \tag{3}$$

where $g=2(1+\alpha/2\pi+\cdots)$ and m/M is the ratio of the mass of the electron to that of the nucleus. This approximation neglects terms of order $\alpha^2 H_{\text{spin}}$ and $(m/M)^2 H_{\text{spin}}$. The factor $(g-1)$ occurs in terms involving the Thomas precession.

The eigenstates of H_0 corresponding to $(1s)(nL)$ Rydberg states are simple products of hydrogenic states

$$\psi(\mathbf{r}_1,\mathbf{r}_2)=\psi_{1s}^{Z=2}(\mathbf{r}_1)\psi_{nLm}^{Z=1}(\mathbf{r}_2)\ . \tag{4}$$

Since H_{Coulomb} is symmetric under interchange of $\mathbf{r}_1$ and $\mathbf{r}_2$, the wave function with the two coordinates interchanged must be an equally good eigenstate. However, because the definition of H_0 is not symmetric, the interchanged function ψ' is not an eigenfunction of H_0 but of H_0' which is obtained from H_0 with a similar interchange of coordinates. This circumstance can be handled through the use of unsymmetric perturbation theory.[8] The properly symmetrized zeroth-order eigenstates can be taken to be the four linear combinations of the product states

$$\psi_{nLS}^0=(2^{-1/2})[\psi+(-1)^S\psi']\,|\,S_1,S_2;S,m_S\rangle\ ,$$

which are eigenstates of $\mathbf{L}=\mathbf{L}_1+\mathbf{L}_2$, $\mathbf{S}=\mathbf{S}_1+\mathbf{S}_2$, and $\mathbf{J}=\mathbf{L}+\mathbf{S}$, namely, ${}^3L_{L+1}$, ${}^3L_L$, ${}^3L_{L-1}$, and ${}^1L_L$. Although these states are not the energy eigenstates of the problem, they do form a convenient basis for calculations.

The first-order perturbation energies due to V and H_{spin} can be calculated using unsymmetric perturbation theory. For V alone the result is

$$\Delta E_V=J_C+(-1)^S K_C\ , \tag{5}$$

where

$$J_C=\langle\psi\,|\,V\,|\,\psi\rangle$$

and

$$K_C=\langle\psi\,|\,V\,|\,\psi'\rangle\ .$$

Both of these integrals can be evaluated using the zeroth-order hydrogenic wave functions. Since the perturbation V is zero for $|\,\mathbf{r}_2\,|\gg|\,\mathbf{r}_1\,|$, the integrals decrease very rapidly with L, as shown in Table I. The first-order Coulomb integral J_C does not contribute to the magnetic

TABLE I. Tabulation of Coulomb and magnetic-fine-structure integrals for $10L$ states. (Values in MHz, with the power of 10 in square brackets.)

State	J_c	K_c	J	K	δ
$10D$	−1.1[3]	4.1[3]	2.1[−1]	−5.4[−1]	6.8[−1]
$10F$	−7.6[0]	2.9[1]	9.9[−4]	−2.9[−3]	5.1[−3]
$10G$	−2.7[−2]	1.0[−1]	2.7[−6]	−8.3[−6]	1.9[−5]
$10H$	−5.4[−5]	2.1[−4]	4.3[−9]	−1.4[−8]	3.9[−8]
$10I$	−6.4[−8]	2.5[−7]	4.3[−12]	−1.5[−11]	4.7[−11]
$10K$	−4.4[−11]	1.7[−10]	2.5[−15]	−8.8[−15]	3.3[−14]

fine structure. The exchange integral K_C does contribute to the magnetic field structure, as we have defined it, but is found to be a rather poor approximation to the total exchange energy in states with $L > 3$.[5] Because of the difficulty of calculating the total exchange energy, and because it makes a relatively small contribution to the high-L magnetic field structure, we choose to parametrize it here and represent the contribution of exchange to the magnetic fine structure by

$$\Delta E_x = (-1)^S V_x \ , \tag{6}$$

where V_x is a parameter to be determined by comparison with experiment.

The matrix elements of $H_{\rm spin}$ can be evaluated using the expansions of the solid spherical harmonics.[11,12] The exact matrix elements between properly symmetrized hydrogenic wave functions are conveniently written in terms of the matrix elements of a simpler effective operator, $H^{\rm BB}_{\rm spin}$, which acts on unsymmetrized wave functions (with electron 2 being the Rydberg electron). The nonzero elements are

$$\langle {}^3L_{L+1} \mid H_{\rm spin} \mid {}^3L_{L+1} \rangle = \langle \psi \mid H^{\rm BB}_{\rm spin} \mid \psi \rangle + \frac{L(6L+7)}{4(2L+3)} J + \frac{3L}{4} K \ , \tag{7}$$

$$\langle {}^3L_L \mid H_{\rm spin} \mid {}^3L_L \rangle = \langle \psi \mid H^{\rm BB}_{\rm spin} \mid \psi \rangle - \frac{J}{4} - \frac{3K}{4} \ , \tag{8}$$

$$\langle {}^3L_{L-1} \mid H_{\rm spin} \mid {}^3L_{L-1} \rangle = \langle \psi \mid H^{\rm BB}_{\rm spin} \mid \psi \rangle - \frac{(L+1)(6L-1)}{4(2L-1)} J - \frac{3(L+1)}{4} K \ , \tag{9}$$

$$\langle {}^1L_L \mid H_{\rm spin} \mid {}^1L_L \rangle = \langle \psi \mid H^{\rm BB}_{\rm spin} \mid \psi \rangle + \delta \ , \tag{10}$$

and

$$\langle {}^1L_L \mid H_{\rm spin} \mid {}^3L_L \rangle = \langle \psi \mid H^{\rm BB}_{\rm spin} \mid \psi \rangle + \frac{\sqrt{L(L+1)}}{4} J \ , \tag{11}$$

where

$$J = \alpha^2 \int_{r_2=0}^{\infty} \int_{r_1=r_2}^{\infty} R^2_{1s}(r_1) R^2_{nL}(r_2) r_1^2 r_2^{-1} dr_1 dr_2 \ , \tag{12}$$

$$K = -\frac{4\alpha^2}{2L+1} \int_0^{\infty} \int_0^{\infty} R_{nL}(r_1) R_{1s}(r_1) R_{nL}(r_2) R_{1s}(r_2) \times \left[\frac{r_<^L}{r_>^{L+1}} \right] r_1 r_2^2 dr_1 dr_2 \ , \tag{13}$$

$$\delta = \alpha^2 \int_0^{\infty} R^2_{1s}(r) R^2_{nL}(r) r^2 dr \ , \tag{14}$$

and

$$H^{\rm BB}_{\rm spin} = \alpha^2 \left[\frac{a_1}{2} \frac{\mathbf{L}_2 \cdot \mathbf{S}_2}{r_2^3} - a_2 \frac{\mathbf{L}_2 \cdot \mathbf{S}_1}{r_2^3} + a_3 \frac{\mathbf{S}_1 \cdot \mathbf{S}_2 - 3(\mathbf{S}_1 \cdot \hat{\mathbf{r}}_2)(\mathbf{S}_2 \cdot \hat{\mathbf{r}}_2)}{r_2^3} \right] \tag{15}$$

with

$$a_1 = (g-1) + 2gm/M \approx 1 + \alpha/\pi + 4m/M \ ,$$

$$a_2 = g/2 \approx 1 + \alpha/2\pi \ ,$$

and

$$a_3 = (g/2)^2 \approx 1 + \alpha/\pi \ .$$

By definition, the operator $H^{\rm BB}_{\rm spin}$ acts on unsymmetrized wave functions $\mid \psi \rangle$ of appropriate L, S, and J formed from functions of the form of Eq. (4). The matrix elements of $H^{\rm BB}_{\rm spin}$, which may be evaluated by elementary means, are given for convenience in Table II.

The entire dependence of the matrix elements of $H_{\rm spin}$ on the wave function of the core electron is contained in the integrals J, K, and δ. For high-L states, these integrals are extremely small, as illustrated in Table I, and consequently the matrix elements of $H_{\rm spin}$ are very nearly equal to the matrix elements of $H^{\rm BB}_{\rm spin}$. For instance, in the $10H$ state the terms proportional to J, K, and δ contribute

TABLE II. Matrix elements of the operators occurring in $H^{\rm BB}_{\rm spin}$.

$$\left[\langle r^{-3} \rangle = \frac{1}{n^3 L(L+1/2)(L+1)} \frac{1}{(1+m/M)^3} \right]$$

	$\frac{\mathbf{L}_2 \cdot \mathbf{S}_2}{r_2^3}$	$\frac{\mathbf{L}_2 \cdot \mathbf{S}_1}{r_2^3}$	$\frac{(\mathbf{S}_1 \cdot \mathbf{S}_2 - 3(\mathbf{S}_1 \cdot \hat{\mathbf{r}}_2)(\mathbf{S}_2 \cdot \hat{\mathbf{r}}_2)}{r_2^3}$
$\langle {}^3L_{L+1} \mid 0 \mid {}^3L_{L+1} \rangle$	$\frac{L}{2}\langle r^{-3} \rangle$	$\frac{L}{2}\langle r^{-3} \rangle$	$\frac{L\langle r^{-3} \rangle}{2(2L+3)}$
$\langle {}^3L_L \mid 0 \mid {}^3L_L \rangle$	$\frac{-\langle r^{-3} \rangle}{2}$	$\frac{-\langle r^{-3} \rangle}{2}$	$\frac{-\langle r^{-3} \rangle}{2}$
$\langle {}^3L_{L-1} \mid 0 \mid {}^3L_{L-1} \rangle$	$\frac{-(L+1)}{2}\langle r^{-3} \rangle$	$\frac{-(L+1)}{2}\langle r^{-3} \rangle$	$\frac{(L+1)\langle r^{-3} \rangle}{2(2L-1)}$
$\langle {}^1L_L \mid 0 \mid {}^1L_L \rangle$	0	0	0
$\langle {}^1L_L \mid 0 \mid {}^3L_L \rangle$	$-\frac{\sqrt{L(L+1)}}{2}\langle r^{-3} \rangle$	$\frac{\sqrt{L(L+1)}}{2}\langle r^{-3} \rangle$	0

to the magnetic fine structure only at the level of 10^{-8}. Physically, $H_{\rm spin}^{\rm BB}$ corresponds to the approximation of treating the electrons as distinguishable and ignoring the spatial extent of the core electron wave function. It may be obtained heuristically from $H_{\rm spin}$ by letting $r_1 \to 0$. This approximate form of the spin fine-structure operators has been used by others[1,7,13,14] and has been named the "Breit-Bethe" approximation by MacAdam and Wing.[13] Apparently, the degree of approximation which it involves has not been previously reported.

The predicted magnetic fine structure in this hydrogenic model (equivalent to the "hydrogenic approximation" of Ref. 6) can be obtained by diagonalizing the matrix given by Eqs. (7)—(11) after adding the (diagonal) exchange energies as given by Eq. (6). The eigenvalues that result are

$$E(^3L_{L-1}) = E_{nL} + \langle {}^3L_{L-1} | H_{\rm spin} | {}^3L_{L-1} \rangle - V_x \quad (16)$$

and

$$E(^3L_{L+1}) = E_{nL} + \langle {}^3L_{L+1} | H_{\rm spin} | {}^3L_{L+1} \rangle - V_x \quad (17)$$

for the two unmixed triplet states, and

$$E(^{\pm}L_L) = E_{nL} + \left[\frac{\langle {}^3L_L | H_{\rm spin} | {}^3L_L \rangle + \langle {}^1L_L | H_{\rm spin} | {}^1L_L \rangle}{2} \right] \pm \left[\left[\frac{\langle {}^3L_L | H_{\rm spin} | {}^3L_L \rangle - \langle {}^1L_L | H_{\rm spin} | {}^1L_L \rangle}{2} - V_x \right]^2 + \langle {}^3L_L | H_{\rm spin} | {}^1L_L \rangle^2 \right]^{1/2} \quad (18)$$

for the two states with $J = L$. The singlet and triplet states are completely mixed if

$$V_x \ll \langle {}^3L_L | H_{\rm spin} | {}^1L_L \rangle .$$

Under this condition, the eigenvalues of the $^{\pm}L_L$ states are insensitive to the value of V_x.

In the calculation of Cok,[6] further corrections to the magnetic structure due to the first-order perturbations of the wave function by the Coulomb perturbation V were evaluated. These effects are quite significant for D and F states, but decrease rapidly with L and are less than 10 kHz for the $10G$ state. Using a relativistic two-body equation, in which the He^+ core is treated as a point particle of appropriate total mass, charge, spin, and magnetic moment, Pilkuhn has calculated additional corrections to the Rydberg magnetic fine structure not included in Ref. 6.[7] These effects are significant for D states but appear smaller than 1 kHz for both the $10G$ and $10H$ states. We note that in the treatment of Pilkuhn, an operator similar to $H_{\rm spin}^{\rm BB}$ occurs, but with recoil corrections [order $(m/M)H_{\rm spin}$] *different* from those that we quote above. Whether additional terms of this order would occur as second-order perturbations in our approach (perhaps due to the inclusion of the mass-polarization operator)[15] or whether the differences reflect the inequivalence of the two models is an open question. The next largest uncalculated contributions to the high-L magnetic fine structure appear to be the terms of order $\alpha^2 H_{\rm spin}$ such as those omitted in making the nonrelativistic reduction of the Breit interaction.

III. EXPERIMENTAL TECHNIQUE

The measurements reported here were obtained using the same microwave-optical resonance technique used recently to measure the electric fine-structure intervals between several $n=10$ helium Rydberg states.[1,16] The apparatus is shown in Fig. 2. A fast beam of helium Rydberg states is prepared by charge exchange from a 11.0-keV beam of He^+ ions in a differentially pumped charge exchange cell containing a few millitorr of argon. Those ions that are not neutralized are deflected out of the beam by the electric field in the initial deflector. Those atoms that form in the $10G$ state are efficiently and selectively detected by resonant laser excitation to the $27H$ state, followed by Stark ionization of the $n=27$ atoms and collection of the resulting ions. Possible background due to atoms initially formed in very highly excited Rydberg states is reduced by Stark ionization in the initial deflection region immediately after neutralization. For $n=10$ Rydberg states, a convenient laser is a fixed-frequency CO_2 laser, whose frequency can be discretely turned

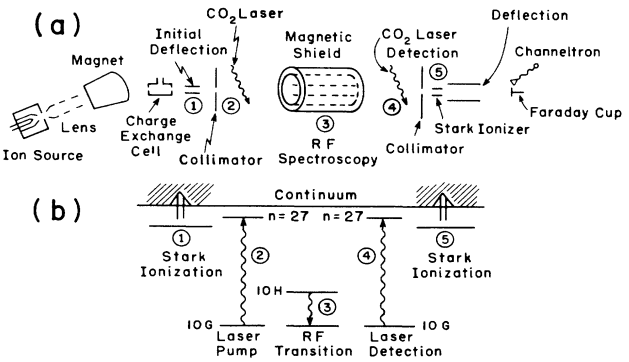

FIG. 2. Experimental setup. A schematic of the atomic beam line is shown in (a). The corresponding atomic levels and transitions are shown in (b). An ion beam is created, focused, bent, and neutralized in the source, lens, magnet, and charge-exchange cell, respectively. Those ions which are not neutralized are deflected out of the beam at (1). At (2), the $10G$ state is depopulated by a CO_2 laser. $10G$ to $10H$ rf transitions are induced at (3). The $10G$ state is once again emptied into the $27H$ state at (4). These $n=27$ atoms are ionized at (5) and the resulting ions detected by a channel electron multiplier.

among a large number of lines in the 9—11-μm wavelength range. Fine tuning of the laser resonance is accomplished with Doppler tuning by varying the angle of intersection between the laser and the fast beam ($v/c = 0.002\,43$). When the laser is tuned to detect atoms in the $10G$ state, the resulting ion current serves to detect microwave-induced transitions between the $10G$ and $10H$ states which occur near 500 MHz. The signal is measured by modulating the microwave power and measuring the synchronous modulation of the ion current for a range of microwave frequencies. Since the signal depends on the initial population difference between the states, its size can be enhanced by depleting the population of the $10G$ state with an additional laser-interaction region before the rf interaction region. The rf transitions are induced in a section of TEM transmission line that is enclosed in a double magnetic shield to eliminate the earth's magnetic field. The transmission line is constructed out of a one-meter length of WR229 (EIA) waveguide with an inner conductor added in such a way as to give a TEM impedance near 50 Ω.[16]

The spectrum of $10G$-$10H$ transitions observed with this scheme depends on the strength of the rf electric field in the transmission line, as illustrated in Fig. 3. There, plotted as a function of the rf frequency, are shown the energy of the four magnetic fine structure levels within the $10H$ manifold (horizontal lines) and the energies that are one rf photon greater than the four magnetic-fine-structure levels of the $10G$ manifold (sloping lines). The intersection point of any two lines represents a possible $10G$-$10H$ resonance frequency, but whether such an intersection leads to an observable resonance depends on the strength of the electric-dipole matrix element connecting the intersecting levels and on the rf electric field amplitude. At relatively low rf field strength ($\simeq$0.004 V/cm) only the four strongest transitions are observed as shown in the upper resonance signal of Fig. 3 and in Ref. 1. At larger rf fields ($\simeq$0.020 V/cm) these four transitions are power broadened and other weaker transitions become visible, as shown in the lower resonance signal of Fig. 3. The positions of the seven resonance transitions indicated by dashed lines have been measured and used to uniquely determine the three magnetic fine-structure intervals within the $10G$ and $10H$ manifolds.

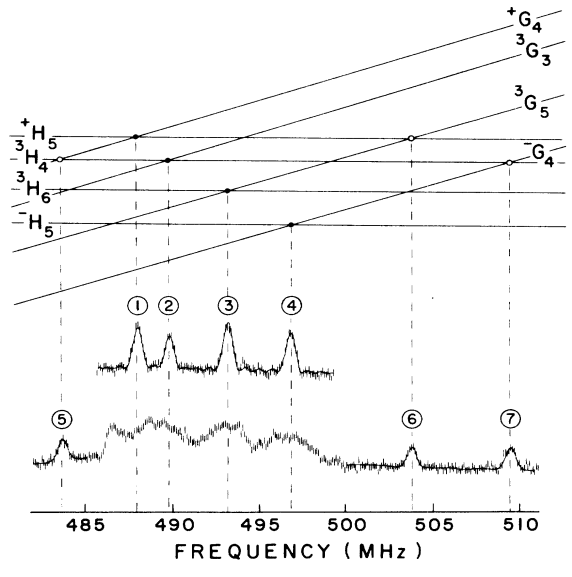

FIG. 3. Level-crossing diagram showing the seven rf resonance features. The upper frequency scan shows the four strongly allowed transitions. The lower scan shows the additional three features which appear at higher rf power. The top part of the figure identifies the peaks, as explained in the text.

IV. MEASUREMENTS

Measurements of resonance positions were carried out by stepping the rf frequency (produced by a Marconi 2019 microwave signal generator) across the resonance curve in 0.1-MHz increments under the control of an Apple IIe microcomputer. The microwave power was square-wave modulated at 1 kHz and the measured signal was proportional to the synchronous component of the collected ion current. This signal was averaged over 30 sec at each frequency, with the result recorded by the microcomputer. A resonance could be automatically scanned in this way in about 6 min. The resulting curve was fit to the function

$$S(\nu)=A+B(\nu-\nu_0)+C\sum_m\left[\frac{\sin(bT/2)}{b}\right]^2 V_m^2 , \qquad (19)$$

where

$$b=2\pi[(2V_m)^2+(\nu-\nu_0)^2]^{1/2} ,$$

$$V_m=\frac{eE}{2h}\langle 10H,J',m\,|\,z\,|\,10G,J,m\rangle ,$$

E is the rf electric field amplitude, T is the transit time through the rf interaction region (1.37 μsec), and A, B, C, and ν_0 are free parameters. This procedure was repeated several times (typically 20) for each peak during each data

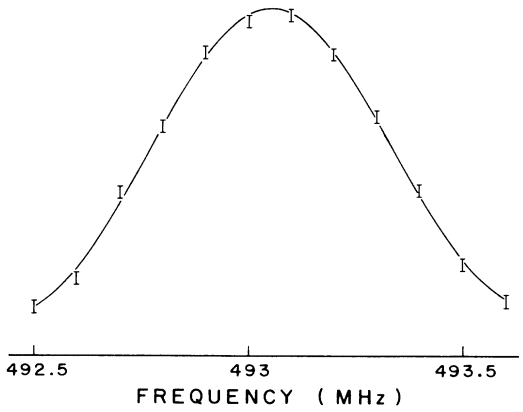

FIG. 4. Measured resonance line shape for peak 3 of Fig. 3, obtained by averaging 20 individual line scans. The smooth curve is the fitted line shape described in the text.

run and the results for each peak were averaged to give the best estimate of peak position. The scatter in the measured line centers for individual line scans was used to compute the statistical errors in the measured positions. The fitted values of the parameters A and B were found to vary systematically among the various peaks, due to the influence of neighboring resonances. Figure 4 shows the average of the measured resonance signals for peak 3 during one data run, together with the fitted line shape. The line position measurement derived from the data illustrated there has a precision of ± 0.006 MHz, which is about 1% of the 650-kHz linewidth.

Precise determinations of the seven resonance positions were obtained through a series of such measurements designed to minimize the influence of the following systematic effects.

(i) *Doppler shifts.* These are present because the rf propagates along the same axis as the fast beam. Since the Doppler shifts can be accurately reversed by changing the direction of rf propagation, they are easily eliminated.

(ii) *Reflected wave shifts.* Whatever the nominal direction of rf propagation, a small reflected wave is also present due to imperfect impedance matching at the exit of the transmission line. Direct measurements show the magnitude of the reflection coefficient to be $|\Gamma| \leq 0.10$. The reflected wave produces a shadow spectrum of order $|\Gamma|^2$ with the opposite Doppler shift, which is too small to be significant here. However, since the reflected wave is coherent with the primary wave, there is also an effect of order $|\Gamma|$, which distorts the resonance line shape and shifts its position slightly.[16] It can be shown that this shift in apparent line center will itself reverse if the direction of rf propagation reverses, provided that the reflection coefficients of the two ends of the interaction region are equal. Under these conditions, any bias in the line position is eliminated in the average over the two Doppler-shift directions. This simple procedure will fail, however, if the two nominally identical ends of the rf-interaction region have slightly different reflection coefficients. Even under those circumstances, averaging over the four measurements with both orientations of the rf interaction region and both directions of rf propagation relative to the beam should eliminate the shift in line center due to the reflection wave. For this reason all the precision line-center measurements were repeated in the four apparatus configurations specified in Table III.

(iii) *dc Stark shifts.* In previous measurements using this technique,[1] stray electric fields of the order 0.1 V/cm were observed within the rf-interaction region, leading to Stark shifts of the transition resonances. In that work, the size of such fields was deduced from observations of the position of the three-photon $10I$-$10M$ resonance, which is very sensitive to electric fields. For the present measurement, we adopt a simpler procedure for dealing with this systematic effect, since, to the extent that all the magnetic-fine-structure levels show similar Stark shifts, the relative positions of the seven resonances are insensitive to a constant electric field and we need know only that all the line positions are measured at the same value of the stray field. As a convenient monitor of this field, we used the position of one of the strong resonances, peak 1 in Fig. 3. During each data run, a period of many hours, we repeatedly measure the position of this peak, interspersing these measurements between measurements of the other six peak positions. Figure 5 shows typical observations of the position of peak 1 over time, and illustrates a slow downward shift in the peak positions, due to the buildup of stray electric fields inside the rf-interaction region. The position of this resonance at zero electric field may be deduced from the beam speed and the measurement of Palfrey[1] to be approximately 485.68 MHz. Since the Stark shift rate of this transition is $\simeq -12$ MHz $(\mathrm{V/cm})^{-2}$, it can be inferred that the rms stray electric field builds up from about 0.05 to 0.10 V/cm during the 40 hours represented by Fig. 5. The smooth curve in Fig. 5 is a fit assuming a smooth exponential stabilization of the electric field with time. It indicates a time constant of about 5 h. Using this curve as a time history of the stray field, the measured positions of peaks 2–7 were corrected to constant peak-1 position by noting the time t at which an individual line was observed and the fitted peak-1 position at that time, $\nu_1(t)$. Then, using the calculated quadratic Stark shift rates of the seven resonances, k_i, the corrected position of peak i was obtained from

$$(\nu_i)^{\mathrm{corr}} = \nu_i^{\mathrm{obs}} - \left[\frac{k_i}{k_1}\right][\nu_1(t) - 486.866(10)(1 \pm \beta)] , \qquad (20)$$

where $\beta = v/c = 0.002\,43$ and the $+$ $(-)$ sign in the last term corresponds to configurations A and B (C and D) of

TABLE III. The four geometries in which line centers were measured. The corrections to the line centers are due to the Doppler shift and the reflected waves from the ends of the interaction region. β is the beam speed and ϵ_a and ϵ_b give the reflected wave shifts due to the two ends of the interaction region. Second-order Doppler shifts have been ignored since their contribution to the individual peak positions is small and their contribution to the magnetic-fine-structure intervals is completely negligible.

Configuration	rf propagation	rf region orientation	Line center
A	copropagating	normal	$\nu_0(1+\beta+\epsilon_b)$
B	copropagating	reversed	$\nu_0(1+\beta+\epsilon_a)$
C	counterpropagating	normal	$\nu_0(1-\beta-\epsilon_a)$
D	counterpropagating	reversed	$\nu_0(1-\beta-\epsilon_b)$

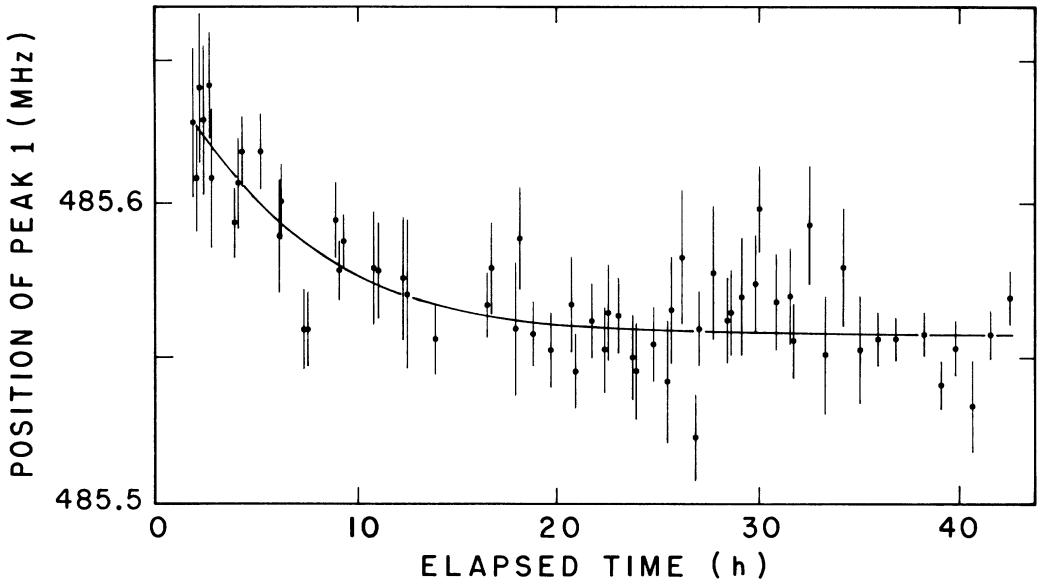

FIG. 5. Position of peak 1 vs time during one data run. The slow downward shift of the peak position is due to the buildup of stray electric fields (of approximately 0.1 V/cm) in the rf-interaction region.

Table III. The corrections to the relative peak positions resulting from this procedure were less than 0.040 MHz. The uncertainty introduced by this procedure is dominated by uncertainty in the relative Stark shift rates and is discussed further below.

Table IV shows the average position of each of the seven resonances obtained in this way from runs in all four apparatus configurations. The best use of all these data is made by fitting them to the expressions

$$\nu(A)_i=\nu_{0i}(1+\beta+c_i\epsilon_b)\ ,$$

$$\nu(B)_i=\nu_{0i}(1+\beta+c_i\epsilon_a)\ ,$$

$$\nu(C)_i=\nu_{0i}(1-\beta-c_i\epsilon_a)\ ,$$

and

$$\nu(D)_i=\nu_{0i}(1-\beta-c_i\epsilon_b)\ ,$$

where $\beta=v/c$ is the beam velocity, ϵ_a and ϵ_b represent the effects of the reflected waves due to ends a and b of the rf-interaction region,

$$c_i=1-k_i/k_1$$

is a constant depending on the relative Stark shift rates of resonance i and resonance 1, $\nu(A)_i$ is the measured position of resonance i in configuration A, and ν_{0i} is the true center of resonance i, free from Doppler shifts, reflected wave shifts, and dc Stark shifts. The parameters ν_{0i} that result from such a fit of the data are shown in the last column of Table IV. They represent the best estimate of the seven peak positions after correcting for the three systematic effects described above. The other fitted parameters that result are $\epsilon_a=0.000\,08(2)$ and $\epsilon_b=0.000\,06(2)$, indicating that the reflected wave effects are about 3% of the Doppler shift and that the difference between the reflection coefficients of the two ends of the rf-interaction region is insignificant. The reduced χ^2 of this fit is 1.17.

Three further systematic corrections must be applied to these measured peak positions.

(iv) *ac Stark shifts.* At the high rf power levels required to observe resonances 5—7, the positions of all the levels are influenced by ac Stark shifts. The shift rates of these

TABLE IV. The measured positions of the seven $10G$-$10H$ resonances in the four geometries of Table III. The averaged positions are given in the last column. (Values are in MHz, with one standard deviation errors in parentheses.)

Peak No.	A	B	C	D	$(\nu_0)_i$
1	488.047(7)	488.040(5)	485.680(4)	485.666(9)	486.863(3)
2	489.909(25)	489.884(7)	487.511(7)	487.523(24)	488.702(5)
3	493.192(10)	493.163(5)	490.765(6)	490.761(24)	491.971(4)
4	496.778(19)	496.757(9)	494.347(6)	494.306(15)	495.552(5)
5	483.580(8)	483.572(4)	481.221(8)		482.396(8)
6	503.870(23)	503.872(9)	501.414(8)		502.645(10)
7	509.664(14)	509.647(8)	507.170(9)		508.411(9)

TABLE V. Systematic corrections to peak positions. This table shows, for each of the seven peaks, the ac Stark corrections and the systematic uncertainties due to line overlap and dc Stark shifts. The final column shows the corrected positions of each peak. (Values are in MHz.)

Peak No.	ac Stark	Line overlap	dc Stark	Corrected position
1	0.000(0)	0.000(2)	0.000(0)	486.863(4)[a]
2	0.000(0)	0.000(2)	0.000(1)	488.702(5)
3	0.000(0)	0.000(1)	0.000(1)	491.971(4)
4	0.000(0)	0.000(1)	0.000(1)	495.552(5)
5	−0.121(7)	0.000(1)	0.000(9)	482.275(14)
6	0.051(3)	0.000(1)	0.000(9)	502.696(14)
7	0.042(2)	0.000(1)	0.000(9)	508.453(13)

[a]By assumption, the position of this peak agrees with Ref. 1.

three resonances can be calculated readily using the approach described in Ref. 17, along with the assumption that all m_J states are equally populated. Since the largest shift occurs in peak 5, the position of that peak was carefully measured at a range of rf powers and extrapolated to zero power. Then, using the relative shift rates, corrections could be applied to all three resonances as shown in Table V. Included in this procedure were small but significant corrections (≤ 0.020 MHz) which account for nonlinearities in the shift rates due to the onset of saturation of each of the m-state resonances.

(v) *Line overlap.* The centers of each of the seven resonances were determined from fits of single peaks, assuming the theoretical line shape given above. This approach ignores the very slight overlap of the line shape from neighboring peaks. We have modeled this overlap and estimated that the uncertainties which result are less than 2 kHz. (See Table V.) One reason this effect is small is that we floated a linear background when fitting our peaks and this partially compensates for these overlap effects.

(vi) *dc Stark shift.* The procedure for dealing with dc Stark shifts by measuring the peak position relative to peak 1 was described above. The limitation of this procedure is the uncertainty in the relative Stark-shift rates of the different peaks. These shift rates depend on the polarization of the stray electric field relative to the polarization of the rf electric field ($\hat{\mathbf{z}}$). Since the shift rates are different for different m states, the average rate also depends on the relative populations of the m states and on the degree of saturation of the rf transitions. A study of these effects indicates that the shift rates of peaks 1—4 are nearly equal under any circumstances, but that the shift rate of peaks 5, 6, and 7 relative to these is a strong function of stray field polarization. Experimental data on the relative positions of peaks 1 and 5 at various times were used to deduce the relative shift rate:

$$k_5 - k_1 = -3.8(7)\ \text{MHz}\,(\text{V/cm})^{-2}\ .$$

This result is consistent with the value predicted for a z-polarized stray field [-4.0 MHz$\,(\text{V/cm})^{-2}$] and quite different from that predicted for an x-polarized stray field [$+1.7$ MHz$\,(\text{V/cm})^{-2}$]. In each case, equal m-state populations and an appropriate degree of saturation were assumed. We therefore adopted the shift rates calculated for a z-polarized stray field for use in Eq. (20), and take each shift rate to be uncertain by 15% of the difference between the calculated rates for z- and x-polarized fields. This leads to the systematic uncertainties for each peak positions as shown in Table V.

The final results for the corrected positions of all seven peaks are shown in column 5 of Table V. Since the position of peak 1, by assumption, agrees with the measurement of Palfrey,[1] the significant results of this experiment are the measured positions of each of the other six peaks relative to peak 1. From these we can deduce the relative positions of each of the magnetic-fine-structure levels in both the $10G$ and $10H$ manifolds. The results are shown in Table VI. Also shown in Table VI are the $10G$ magnetic-fine-structure splittings as derived from measurements of the $10D$-$10G$ transition energies by MacAdam and Wing,[18] and deduced from the global fitting formulas given in Farley *et al.*[19] The agreement with these earlier, less precise measurements is satisfactory. In the case of the $10H$ state, or any other state with L greater than 4, no previous measurements exist.

V. DISCUSSION OF RESULTS

Table VII compares the measured magnetic fine structure with theory. In view of the difficulties in accurately calculating the total exchange energy,[5] we regard V_x as a free parameter for both the $10G$ state and the $10H$ state and choose the value that gives the best agreement between theory and experiment. In column 2 are shown (as a function of V_x) the magnetic-fine-structure predictions derived from Eqs. (16)—(18). These predictions neglect

TABLE VI. Measured values of the $10G$ and $10H$ magnetic-fine-structure intervals. (Values are in MHz.)

Interval	This work	MacAdam and Wing[18]	Farley *et al.*[19]
$^{+}G_4$-$^{-}G_4$	26.178(14)	25.84(51)	26.27(14)
$^{3}G_3$-$^{-}G_4$	19.755(14)	19.58(53)	19.92(17)
$^{3}G_5$-$^{-}G_4$	10.345(20)	10.39(68)	10.54(26)
$^{+}H_5$-$^{-}H_5$	17.489(15)		
$^{3}H_4$-$^{-}H_5$	12.905(14)		
$^{3}H_6$-$^{-}H_5$	6.764(22)		

TABLE VII. Comparison between theory and experiment for the magnetic fine structure of helium $10G$ and $10H$ states. (Values are in MHz.)

Interval	This expt.	Eqs. (16)—(18)	With Ref. 6 corrections
${}^{+}G_4$-${}^{-}G_4$	26.178(14)	26.168	26.166
${}^{3}G_3$-${}^{-}G_4$	19.755(14)	$19.828-V_x$	$19.821-V_x$
${}^{3}G_5$-${}^{-}G_4$	10.345(20)	$10.393-V_x$	$10.394-V_x$
	best fit $V_x(10G)$:	0.065(11)	0.060(11)
	reduced χ^2:	0.78	0.61
${}^{+}H_5$-${}^{-}H_5$	17.489(15)	17.477	17.477
${}^{3}H_4$-${}^{-}H_5$	12.905(14)	$12.897-V_x$	$12.897-V_x$
${}^{3}H_6$-${}^{-}H_5$	6.764(22)	$6.763-V_x$	$6.763-V_x$
	best fit $V_x(10H)$:	$-0.006(12)$	$-0.006(12)$
	reduced χ^2:	0.36	0.36

any nonhydrogenic part of the wave function which might be produced by the Coulomb perturbation V. Agreement with the measured intervals is satisfactory for both the $10G$ and $10H$ states with suitable choices of V_x in the two cases. Including the corrections due to the first-order Coulomb perturbations of the wave function, calculated by Cok[6] and shown in column 3 of Table VII, gives no significant change for the $10H$ state, but slightly improves the agreement for the $10G$ state. We conclude that for both states the magnetic fine structure is consistent with theory at the 10^{-3} level, in contrast to the rather poor agreement at high L noted by Cok.[6] In addition to confirming the $\alpha H_{\rm spin}$ corrections due to the anomalous moment, this supports Cok's prediction that the structure approaches a simple limit at high L.

The best values for the exchange energies derived from the fits of the magnetic structure are

$$V_x(10G)=0.060(11)\ \text{MHz}$$

and

$$V_x(10H)=-0.006(12)\ \text{MHz}\ .$$

Chang and Poe have calculated total exchange energies for these states of 0.032 and 0.000 MHz, respectively.[5,20] Agreement is satisfactory for the $10H$ state, but rather poor for the $10G$ state.

We expect that, with continued work, it should be possible to measure these magnetic-fine-structure intervals much more precisely with the techniques described here. If the systematic problems can be overcome, the limit set by the natural width of the states would make measurements at the 10^{-5} level of precision a reasonable goal. Such measurements would allow a detailed test of contributions of order $\alpha^2 H_{\rm spin}$ which are presently uncalculated and which must be derived from a more fundamental theory.[21] This test would complement the careful comparison of theory and experiment that has already been carried out for the fine structure of the $2\,{}^3P$ state of helium,[22] since in the high-L states a sufficiently precise Coulomb wave function is rather easily obtained. For instance, a comparison between columns 2 and 3 of Table VII indicates that the magnetic fine structure of $n=10$ helium Rydberg states with $L>4$ can be described to a precision of 10^{-4} using the zeroth-order hydrogenic wave function. In contrast, achieving comparable precision in the magnetic fine structure of the $2\,{}^3P$ state requires a variational wave function with more than 250 terms.[23] The difference stems from the fact that the actual two-electron Rydberg-state wave function is very close to the simple hydrogenic form. Thus studies of this magnetic structure with a precision of 10^{-5} offer a unique opportunity to test aspects of a fully relativistic theory of the helium atom in states with very simple wave functions.

ACKNOWLEDGMENTS

We are greatly indebted to Stephen L. Palfrey for his work in developing the experimental technique used here. This work was supported by National Science Foundation under Grant No. PHY84-13123.

[1]S. L. Palfrey and S. R. Lundeen, Phys. Rev. Lett. **53**, 1141 (1984).

[2]C. K. Au, G. Feinberg, and J. Sucher, Phys. Rev. Lett. **53**, 1145 (1984).

[3]This notation agrees with Ref. 1 but disagrees with the (equally arbitrary) convention of D. R. Cok and S. R. Lundeen, Phys. Rev. A **19**, 1830 (1979); **24**, 3283 (1981), which denotes the states by ${}^{1,3}L$ even after the total spin quantum number has no meaning.

[4]R. J. Drachman, Phys. Rev. A **31**, 1253 (1985).

[5]T. N. Chang and R. T. Poe, Phys. Rev. A **10**, 1981 (1974).

[6]D. R. Cok and S. R. Lundeen, Phys. Rev. A **19**, 1830 (1979); **24**, 3283 (1981).

[7]M. Martinis and H. Pilkuhn, J. Phys. B **15**, 1797 (1982).

[8]H. A. Bethe and E. E. Salpeter, *Quantum Mechanics of One- and Two-Electron Atoms* (Plenum, New York, 1977).

[9]R. A. Hegstrom, Phys. Rev. A **7**, 451 (1973).

[10]M. Douglas, Phys. Rev. A **6**, 1929 (1972). Note that certain terms of order m/M which are nonzero only for p states have been omitted.

[11]R. A. Sack, J. Math. Phys. **5**, 252 (1964).

[12]R. K. Van den Eynde, G. Wiebes, and Th. Niemeyer, Physica

59, 401 (1972).
[13]K. B. MacAdam and W. H. Wing, Phys. Rev. A **12**, 1464 (1975).
[14]H. A. Bethe, *Handbuch der Physik*, 2nd ed., edited by H. Geiger and K. Scheel (Springer, Berlin, 1933), Vol. XXIV/1, p. 380.
[15]L. Hambro, Phys. Rev. A **5**, 2027 (1972).
[16]S. L. Palfrey, Ph.D. thesis, Harvard University, 1983 (unpublished).
[17]J. R. Brandenberger, S. R. Lundeen, and F. M. Pipkin, Phys. Rev. A **14**, 341 (1976).
[18]K. B. MacAdam and W. H. Wing, Phys. Rev. A **15**, 678 (1977).
[19]J. W. Farley, K. B. MacAdam, and W. H. Wing, Phys. Rev. A **20**, 1754 (1979).
[20]T. N. Chang (private communication).
[21]M. Douglas and N. M. Kroll, Ann. Phys. **82**, 89 (1974).
[22]A. Kponou *et al.*, Phys. Rev. A **24**, 264 (1981).
[23]C. Schwartz, Phys. Rev. **134**, A1181 (1964).